Int. J. Appl. Math. Comput. Sci., 2014, Vol. 24, No. 1, 33–47
DOI: 10.2478/amcs-2014-0003

RECOGNITION OF ATHEROSCLEROTIC PLAQUES AND THEIR EXTENDED DIMENSIONING WITH COMPUTERIZED TOMOGRAPHY ANGIOGRAPHY IMAGING

TOMASZ MARKIEWICZ [*,**], MIROSŁAW DZIEKIEWICZ [***], MAREK MARUSZYŃSKI [***], ROMANA BOGUSŁAWSKA-WALECKA [****], WOJCIECH KOZŁOWSKI [**]

[*] Institute of Theory of Electrical Engineering, Measurement and Information Systems
Warsaw University of Technology, Politechniki 1, 00-661 Warsaw, Poland
e-mail: markiewj@wp.pl

[**]Department of Pathomorphology
Military Institute of Medicine, Szaserów 128, 04-141 Warsaw, Poland
e-mail: wojciechkozlowski@interia.pl

[***]Department of Vascular and Endovascular Surgery
Military Institute of Medicine, Szaserów 128, 04-141 Warsaw, Poland
e-mail: dziekiewicz@wp.pl, maruszynski@interia.pl

[****]Department of Radiology
Military Institute of Medicine, Szaserów 128, 04-141 Warsaw, Poland
e-mail: boguslawska@poczta.onet.pl

In this paper the authors raise the issue of automatic discrimination of atherosclerotic plaques within an artery lumen based on numerical and statistical thresholding of Computerized Tomography Angiographic (CTA) images and their advanced dimensioning as a support for preoperative vessel assessment. For the study, a set of tomograms of the aorta, as well as the ilio-femoral and femoral arteries were examined. In each case a sequence of about 130–480 images of the artery cut-off planes were analyzed prior to their segmentation based on morphological image transformation. A crucial step in the staging of atherosclerotic alteration is recognition of the plaque in the CTA image. To solve this problem, statistical and linear fitting methods, including the least-squares approximation by polynomial and spline polynomial functions, as well as the error fitting function were used. Also, new descriptors of atherosclerotic changes, such as the lumen decrease factor, the circumference occupancy factor, and the convex plaque area factor, are proposed as a means of facilitating preoperative vessel examination. Finally, ways to reduce the computational time are discussed. The proposed methods can be very useful for automatic quantification of atherosclerotic changes visualized by CTA imaging.

Keywords: computed tomography, atherosclerotic plaque, image processing, approximation.

1. Introduction

Visual inspection of atherosclerotic changes, based predominantly on 2D and 3D Computerized Tomography Angiography (CTA) imaging, plays a significant role in vascular surgery. Obviously, during the planning of vascular procedures involving endovascular and hybrid operations, precise recognition of the indications and contraindications strictly determined by the pathology associated with the vascular tree is necessary. Calibrations of an aortic stentgraft or a peripheral stent are crucial for the choice of the surgery type. Robust geometric characterization of the ilio-femoral area may play an important role in the understanding of the impact of the geometric factors on the origin and progression of the vascular disease. The extent of atherosclerotic alteration and automation of its inspection in the peripheral vessels may help to make an optimal treatment decision and pay attention to critical locations in the arterial tree.

This process can be divided into three main steps: recognition of the vessels (the lumens with plaques),

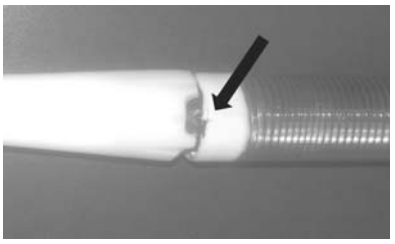

Fig. 1. Sample of the delivering system with a clearly visible broken collar (black arrows) after usage in an endovascular intervention.

plaque detection, and parametrization of the detected abnormalities. The recognition of the vessels can be accomplished using the mathematical morphology and artery tracking algorithm to provide data for the next step of the analysis. In this study we focus on problems associated with the detection of plaques as well as numerical description of the plaque and the lumen in the context of endovascular intervention. Proper artery evaluation can protect against some complications, e.g., a damage to a stent graft delivery system caused by the atherosclerotic plaques, as shown in Fig. 1.

Accurate discrimination between an artery lumen and a calcified plaque allows quantifying atherosclerotic changes. Currently, most systems of artery analysis use fixed threshold values for the whole artery tree to distinguish between the lumen and the plaques based predominantly on colour visualization (e.g., 3DMensio). This approach is simple and seems to be efficient in terms of the time of computation, but its precision is significantly limited. Hence, a more advanced method is needed for the plaque quantification. Renard and Yang (2008) applied the Gaussian mixture model to coronary artery extraction and identification of soft plaques based on CT images. Unfortunately, the authors presented their results only in graphical form, without providing any numerical values. A semi-automatic method of segmentation of the artery wall and the plaque in in-vitro vascular MR images was presented by Yang *et al*. (2003). Adame *et al*. (2004) applied model-based segmentation using contour detection and fuzzy clustering to MR images, and developed an automatic plaque segmentation and characterization in the atherosclerotic carotid artery. A further improvement of the automatic analysis of a plaque in this artery based on MR images was also reported by Kerwin *et al*. (2007). Fuzzy clustering can be also applied for the detection of the retinal artery tree (Yang *et al*., 2008), for the segmentation task in endoscopic colour images (Frąckiewicz and Palus, 2011) and in many other cases of medical imaging.

Segmentation of an artery wall and the dimensioning of plaques based on CTA has also been extensively discussed in the literature. In one study (Manniesing *et al*., 2006), a bone mask obtained from non-contrast registration, user-defined seed points as the volumes of interest, a speed function, and a level set evolution method were used for 3D analysis of the cerebral arteries. In addition, multiple Gaussian distribution modeling (as a base of the speed function) was used to find the optimal threshold value. A fully automatic modification of the above algorithms with the use of the entropy measure and the Hough transform was proposed in another publication by these authors (Manniesing *et al*., 2008). They also proposed an approach based on path tracking with the cost function with the FWMH criterion (Manniesing *et al*., 2010). Generally, all these approaches focus on segmentation of the artery lumen.

Localization of the calcified region in CTA imaging of the carotid artery was analyzed by Vukadinovic *et al*. (2010). Based on the preselected HU range, the candidate object was extracted to find the calcified regions. Feature descriptors and the GentleBoost classifier were applied to recognize the calcification with a 91% accuracy. The outer vessel wall segmentation obtained by these authors is unique and commendable. Also, in this study, CTA-based automated segmentation of the atherosclerotic carotid plaque volume and components was statistically compared with the manual results. However, none of these studies have aimed at comparing different regions of the peripheral vessel tree.

Based on the analysis of the ilio-femoral region visualized by CTA, we discovered a specific distribution of the sorted pixel intensities. In this sorted sequence, the border between the lumen and the plaque is seen as a bending point on the distribution curve. A range of the nearly horizontal distribution curves represents the lumen pixels while a range with a highly increased slope refers to the plaque area. In the present study check this hypothesis for the aorta and the femoral arteries. The results indicate that the hypothesis is true for the aorta, but in the femoral arteries the distribution curve is more variable and has a steeper slope, also for the lumen area. To illustrate the distribution of the pixel intensities in the aorta, the ilio-femoral and the femoral arteries (some examples) are shown in Fig. 2.

In the present paper we compare numerical and statistical approaches to the problem of thresholding atherosclerotic plaques. Based on the assumption that the values of the pixels from our image represent multimodal density, we used Gaussian Mixture Models (GMMs) thresholding as the statistical method (Demirkaya *et al*., 2009). After verification on the arteries of the ilio-femoral region, we found that other popular methods such as Otsu, the minimum error, or clustering are not useful for this purpose. The original idea of the present study consists in the use of numerical methods of linear fitting. These methods allow detecting bending points on the distribution curves based on the analysis of the derivatives.

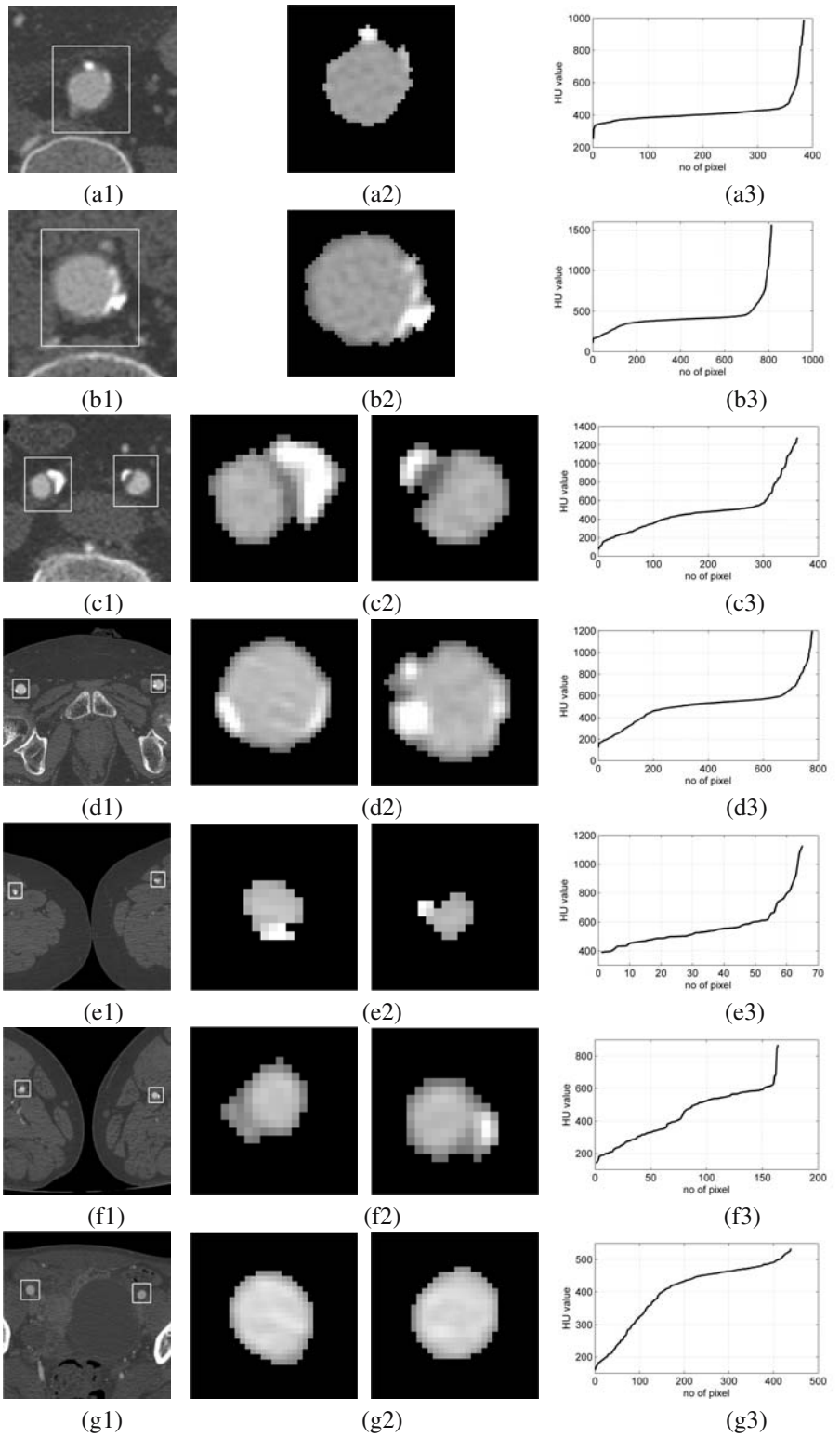

Fig. 2. Examples of the CTA images (1), extracted artery areas (2), and their intensity distribution curves (3). Cases (a) and (b) represent the aorta region, (c) and (d)—the ilio-femoral region, and (e) and (f)—the femoral region of the vessel tree. Case (g) illustrates healthy arteries without calcified plaques.

The applicability of these methods for the examination of three different arteries (aorta, ilio-femoral, and femoral) as well as the analysis of the computational time are presented.

After discrimination between the lumen and the plaque, numerical descriptors of both should be applied to support the diagnosis and treatment. We propose a set of measures based on the presence of the plaque, its space distribution and the surface of the artery lumen. The descriptors of the decrease of the lumen area and the circumference occupancy by the plaque as well as of the maximal elliptic area of the lumen are proposed and discussed here.

2. Material and methods

2.1. Material. The investigated recognition methods were evaluated based on ten tomograms of three arterial regions: the aortic, the ilio-femoral, and the femoral region. CTA images were obtained from patients with different stages of atherosclerosis. The patients were candidates for the endovascular or open surgery at the Department of Vascular and Endovascular Surgery, Military Institute of Medicine in Warsaw. Only the arteries whose lumens were continuous on multi-slice CT imaging were included in the investigation, while those with occlusions or aneurysms were disregarded. All images were obtained using a 64-slice General Electric (Fairfield, CT, USA) MSCT. Each CTA was performed with a standardized optimized contrast-enhanced protocol (120 kVp, 180 mAs, collimation 64×0.625 mm, pitch 0.5). All the patients were injected with 150 ml of the contrast medium (Iomeron Bracco, UK, 400 mg/ml) with SmartPrep. The obtained images were reconstructed for the 250-mm field, 512×512 matrix size, 0.625 mm slice thickness, 0.625 increment, with the standard reconstruction filter applied. The obtained CT images were stored in the DICOM format ver. 3. The actual number of images depended on the investigated region and anatomical conditions of the patient. Average image numbers for the aorta, the ilio-femoral artery, and the femoral artery were 132, 236, and 483, respectively. Thus, the total numbers of the analyzed images equalled 1324, 2359, and 4833, respectively.

2.2. Artery recognition and tracking. In the analysis of the spatial arrangement of arteries visualized with the use of a contrast agent, the artery lumen (filled with blood and the contrast medium) is expected to be lighter than the artery wall and the nearby organs (only atherosclerotic plaques and the bone will be lighter than the artery lumen). This suggests that appropriate recognition of the artery planes relies on the extraction of the locally lighter regions from the image. To achieve this aim, we use a mathematical morphology operation such as extended regional maxima (Soille, 2003). With this transformation, any object with the intensity value higher than those of the borders by at least a selected threshold (in this case 40) can be extracted. We noted that the application of the extended regional maxima can extract the artery lumens with atherosclerotic plaques on their borders that have higher intensities than the regular artery lumens.

To select artery planes in a CTA image after the extended regional maxima transformation, we built a tracking algorithm starting from the point of division of the femoral artery into its superficial and deep branches. This starting point must be selected manually on the artery area by marking the planes of the left and the right artery. The same is required for the algorithms used by other authors (e.g., Manniesing *et al*., 2007; Vukadinovic *et al*., 2012). The markings are then used to select the appropriate objects (segmented by a morphological operation) on the artery planes in subsequent CTA images. An analysis of the next image in the CTA sequence is performed by the extended regional maxima transformation and filtered by the opening and closing transformations. The binary image thus obtained shows not only the markers in the artery areas, but also other separate objects such as bones and smaller arteries. To select the artery planes, the previous image is used as a reference for reconstruction of the appropriate objects. The artery areas extracted from any slide form the basis for the analyses presented in this paper.

2.3. Plaque recognition. One of the crucial steps in computerized evaluation of atherosclerosis is recognition of the plaques in CTA images. Appropriate detection of the plaque area affects each measure used by us as well as qualification for endovascular intervention. In this study we took into account both the statistical and linear fitting methods which are based on a completely different interpretation of the image data. The main ideas of the investigated methods are described briefly in the following section.

2.3.1. Statistical methods. The first group of the investigated methods used for image thresholding consisted of between class variances, minimum error thresholding, K- and C-means clustering as well as mixture-modeling-based thresholding. All these methods are well recognized and have been previously used in different applications of image processing (Demirkaya *et al*., 2009). However, the variable number of classes present in the image, their disproportionality and distribution significantly restrict the utility of these methods. Since only the mixture-modeling-based thresholding yielded acceptable results, we utilized this method in the present study. It is based on the assumption that pixel values covering the examined area in the

image represent multimodal density. The mode is a data value whose frequency is not less than the frequency of neighbouring values. In practice, the modes are identified as peaks in the histogram. They correspond to certain regions of the image when the number of pixels attaining those values is relatively high. By identifying the probability density function (*pdf*) of the pixel values, we can define the probability of any pixel value belonging to different classes (modes) or regions of the image. Let x be a pixel value and $f(x)$ its *pdf*, which can be roughly estimated as the frequency of occurrence of the grey level in the histogram of the image. If we have k modes (classes) in the *pdf* of the pixel values, we may say that x may come from any of those k classes with a different probability. This means that the multimodal multivariate *pdf* function $f(x)$ can be expressed as (Demirkaya *et al*., 2009)

$$f(x) = \sum_{i=1}^{k} \omega_i f_i(x|\Theta_i), \tag{1}$$

where ω_i is the prior class probability of the i-th component of *pdf* and $f_i(x|\Theta_i)$ represents the class conditional *pdf* of pixel x associated with a set of parameters Θ_i. If we assume the Gaussian components in our model, we can represent $f_i(x|\Theta_i)$ as a multivariable normal *pdf* (Demirkaya *et al*., 2009),

$$f_i(x|\Theta_i) = N(x|\mu_i S_i), \tag{2}$$

where μ_i is the $d \times 1$ mean vector and S_i is the $d \times d$ covariance matrix.

However, it should be noted that the choice of using a normal distribution in the mixture model may or may not be appropriate, depending on how the histogram looks. The most favourable situation is when each class has a normal distribution and the histogram can be precisely decomposed into a set of normal distribution parts. Unfortunately, in the problem under study, the distribution of the pixel intensities is close to normal only in the lumen area. If the artery slide includes calcified plaques, the right part of the histogram related to these plaques has a totally different distribution. In this case, the convergence of the optimization algorithm towards the expected solution depends on the domination of the lumen pixels in the data set. For the solution of the Gaussian mixture modeling, the log-likehood function is defined as

$$L(\Theta) = \log \prod_{j=1}^{n} f(x_j|\Theta) = \sum_{j=1}^{n} \log f(x_j|\Theta). \tag{3}$$

The practical way to estimate the unknown parameters Θ of a mixture model is to select them in a way that maximizes the log-likehood function. Thanks to the logarithm transformation, finding the maximum is usually much simpler and can be done numerically using various optimization algorithms. We used implementation based on the Expectation Maximization (EM) iterative method. The initialization of the classes is usually brought about by applying K-means clusterization. Compared with random initialization, such clusterization improves the convergence of the EM algorithm. After the initialization, the expectation of the posterior probability that an observation belongs to a specific class and the maximization of the likelihood function are used one by one in the iterative process. Once a mixture model is fitted to image *pdf*, we can assign pixels to different classes on the basis of the final estimated posterior probabilities, i.e., assigning the pixel x_j to the class that produces the highest value of probability $P(\Theta_i(x_j))$. The details of this approach can be found in the work of Demirkaya *et al*. (2009). This method of segmentation we will henceforth call the Gaussian mixture model.

As shown in Fig. 2, some pixel intensity distributions include a fixed component which significantly restricts the proper Gaussian modeling of the data. The cases in which the fixed component is included are limited mainly to the imaging of narrow arteries, e.g., in the femoral region, as indicated in Fig. 2. Elimination of this component from the distribution curve should increase the accuracy. However, statistical determination of this fixed component is very complicated due to the unstable character of the curve and its local slope variability. As an alternative, prior to the use of the GMM, in our study we applied the linear regression model to eliminate the potentially existing fixed component.

A primary question in GMM application is how many classes exist in the data set. Let us consider the division of an artery plane into three classes: the lumen, the calcified plaques, and the non-calcified plaques. If the variance of the pixels belonging to the class of the largest mean is smaller than 3,000, then the calcified atherosclerotic plaques are not present in this region and all the pixels represent the artery lumen (i.e., only one class region). The value of 3,000 was chosen as most accurate based on the set of the tested images (i.e., 56 images representing different regions of the vessel tree obtained from 8 tomograms). Otherwise, pixels of this class represent the calcified atherosclerotic plaques. In the latter cases the variance of the pixels belonging to the class of the next largest mean should be estimated and two possibilities considered: (a) the artery area contains only the lumen and the calcified plaques, and (b) the artery area contains the lumen, the calcified plaques and the non-calcified plaques. In case (a), the middle class can represent either the lumen or the calcified plaque area. When the variance of the pixel intensity is greater than 10,000, it represents the calcified plaque; when it is less than 10,000, it refers to the lumen area. When the middle class represents the plaque area, the class of the

lowest mean represents the lumen. However, when the middle class is interpreted as the lumen, the class with the lowest mean value should be statistically evaluated and then recognized either as the lumen or the non-calcified atherosclerotic plaque area, according to the variance of the latter.

2.3.2. Linear fitting methods. Analysis of the shape of the distribution curve allows us to hypothesize that its parts with different slopes represent specific cut-off areas of the artery: the lumen and the calcified plaques. A bending point of that curve probably well indicates the border between intensities of the pixels representing the recognized regions. This observation suggests that detection of bending points can be suitable for the thresholding of the pixel intensities for artery cut-off area segmentation into the lumen and the calcified plaques. The bending point should be localized as the first point on the right side of the curve with a value of the derivative (first or second) lower than the selected level. This approach was used by us for each linear fitting method. The task is converted into the analysis of the derivative(s) of the curve. However, numerical calculation of the derivative based on the finite difference methods or a differential rule (e.g., the Gear rule) cannot adequately solve this problem due to the influence of the local variability of curve values. Before the calculation of the derivative, linear fitting should be applied.

In the present study we used the following linear fitting methods: polynomial approximation, various spline-family methods, the piecewise cubic Hermite interpolating polynomial, and the error fitting function. These methods are described briefly in the following section.

Least-square approximation by the polynomial function. One of the simplest methods of linear fitting is least-squares approximation by the fixed degree polynomial. The benefits of this method include a simple function form, a unique system of linear equations used to calculate the function coefficients, and easy determination of the derivatives. The polynomial in the form

$$p(x) = a_n x^n + a_{n-1} x^{n-1} + \cdots + a_1 x^1 + a_0 \qquad (4)$$

has the first derivative

$$\frac{\mathrm{d}p(x)}{\mathrm{d}x} = n a_n x^{n-1} + n - 1 a_{n-1} x^{n-2} + \cdots + a_1 \qquad (5)$$

also in the polynomial form obtained directly from the previously calculated coefficients.

Analysis of the type of the observed distribution curves leads to the conclusion that a low degree polynomial can be inadequate for linear fitting of the data due to the presence of long linear sections of the curves. Simultaneously, increasing the degree worsens the conditioning of the linear equation system. In practice, we used the 12-th degree polynomial function as a suboptimal solution. The threshold is defined as four times the polynomial derivative taken from the right side of the curve. This value was selected in the initial test based on complete slide sequences for ten patients. The examined values of the derivatives were from 2 to 6 with the step of 0.2 and the minimum plateau on the curve was from 4 to 5 (2.2–2.3% of MAE). The value of 4 was selected as the minimum false negative which protects against underestimating the plaque area.

Spline polynomial function. The spline technique has been widely applied for problems with a large number of interpolation data or knots in the approximation task. A solution to the interpolation task is usually defined as the spline function set from sub-intervals of the third-degree polynomials (Stoer and Bulirsch, 2010),

$$S_{[x_i, x_{i+1}]}(x) = a_0^{(i)} + a_1^{(i)} x + a_2^{(i)} x^2 + a_3^{(i)} x^3. \qquad (6)$$

The spline function should have a continuous derivative up to the second degree and knots in all the data points. This type of spline will be called cubic spline interpolation and we will use its second derivative to define the intensity threshold value. Based on the preliminary tests, we set the value of the second derivative at 0.5. It should be noted that this solution is very sensitive to the local variability of the curve values may sometimes produce an inflated value of the threshold. This can result in undersegmentation of the calcified plaque. The value of 0.5 was selected in the same way as in the previous method.

In order to avoid the influence of local data variability, we can use the smoothing of the data. The smoothing can be performed with an averaging filter of size 8. This can be a useful procedure before application of the linear fitting method without the averaging of the data inside the algorithm. Results of the data preprocessing are shown in Section 3.

The linear fitting can also be defined in the approximation task by the B-form of *least-squares spline approximation* with the set of knots. The distance of the function f from the given data y_j which represent the values for $j = 1, 2, \ldots, n$ of the n-th abscissae x_j is measured by

$$E(f) = \sum_{j=1}^{n} \omega_j |y_j - f(x_j)|^2 \qquad (7)$$

with the default choice of weights ω making $E(f)$ the composite trapezoidal rule approximation. When the number of the knots is lower than that of the data, data points which are similarly related to the knots are replaced by their average.

A more sophisticated form of least-squares spline approximation is the *smoothing spline* (De Boor, 2001). The smoothest means that the following functional is minimized:

$$F(D^m f) = \int_{\min(x)}^{\max(x)} \lambda(t)|D^m f|^2 \,\mathrm{d}t, \tag{8}$$

where $D^m f$ denotes the m-th derivative of f and λ is a smoothing parameter. When one uses the second derivative and λ as the constant value of 1, this formula transforms into the cubic smoothing spline.

There are at least two variants of smoothing splines. The first one minimizes $F(D^m f)$ over all f functions for which the error measure $E(f)$ is no bigger than the given tolerance (e.g., 0.5). The second one, by introducing the smoothing parameter ρ and the converted aim function, is defined as

$$\rho \sum_{j=1}^{n} \omega_j |y_j - f(x_j)|^2 + (1-\rho) \int \lambda(t)|D^2 f(t)|^2 \,\mathrm{d}t. \tag{9}$$

The summing is done through the entries of x with the weight function ω and the piecewise constant weight function λ, both selected as constant functions equal to 1. Furthermore, $D^2 f$ denotes the second derivative of the function f and ρ is the smoothing parameter.

Another approach in the spline family is the *Piecewise Cubic Hermite Interpolating Polynomial (PCHIP)* (Fritsch and Carlson, 1980). This method is based on spline functions in the Hermite polynomial form of the third order. This interpolation is realized for each subinterval between the sequential data points with satisfying their values and the continuity of the tangents. For the unit interval $x \in [0,1]$ the interpolation polynomial can be defined as

$$\begin{aligned} p(x) =& (2x^3 - 3x^2 + 1)y_0 + (x^3 - 2x^2 + x)M_0 \\ &+ (-2x^3 + 3x^2)y_1 + (x^3 - x^2)M_1, \end{aligned} \tag{10}$$

where y_0, y_1 are given values of the interval border points and M_0, M_1 are the relevant moments. The moments are chosen in such a way that $p(x)$ preserves the shape of the data and respects monotonicity. If the data are not smooth, a practical effect of PCHIP application is that it has no overshoots and oscillates less.

Another significant point in the linear fitting task is the basic spline function (*B-splines*). This function of the k-th degree for the given knots K is defined as

$$f(x) = \sum_{j=0}^{n} B_{j,k}(x, K) y_i, \tag{11}$$

where $B_{j,k}$ is the j-th basic function degree k.

An extension of the B-spline is the Non-Uniform Rational Basis Spline (NURBS) (Piegl and Tille, 1997). However, in our case there is no way to differentiate between the weights of the data points.

Error function fitting. A monotonous (although not strictly) character of the pixel intensity distribution line may serve as a starting point for the next method. Imposition of such a restriction on the solution may lead to better results of the linear fitting of the examined data. Here, our approach is based on a set of error functions (Andrews, 1997). In mathematics, the error function (also called the Gauss error function) is a non-elementary sigmoidal function defined as

$$\mathrm{erf}(x) = \frac{2}{\sqrt{\pi}} \int_0^x e^{-t^2} \,\mathrm{d}t. \tag{12}$$

When x is negative, the integral is interpreted as the negative of the integral range from x to zero. In practice, the error function of the negative argument value is calculated for its opposite and obtained with a minus.

To the linear fitting, we build the set of $C_i(x)$ functions for $i = 1, 2, \ldots, k$ in such a away that

$$C_i(x) = \mathrm{erf}(\frac{x - K_i}{\sigma}), \quad \sigma = \frac{\sqrt{2}}{k}(x_n - x_0), \tag{13}$$

where x_0, x_n are the interval bordering points and k is a number of knots K. In this case, the following conditions occur:

- all $C_i(x)$ functions are monotonously in the x range;
- the first function $C_1(x)$ has a value between 0 and 1, the last $C_k(x)$ has a value between -1 and 0;
- the rest of the $C_i(x)$ functions have values closely to the range $[-1, 1]$ with the bending point at an appropriate knot with a value equal to 0.

The solution of the linear fitting can be obtained by solving the constrained linear least squares problem. The set of $C_i(x)$ functions is supplemented with a bias value and a linear function, and the solution of linear fitting $f(x)$ can be expressed as

$$f(x) = \mathrm{bias} + a_0 x + \sum_{i=1}^{k} a_i C_i(x). \tag{14}$$

The linear least squares problem has lower constraints on coefficients $a_0, a_1, \ldots, a_k$ in the form of zero values. This assumption allows obtaining the solution in monotonic form.

2.4. Descriptors of atherosclerotic changes. One of the most important practical aspects of plaque recognition is evaluation of the atherosclerotic alterations in the artery prior to endovascular intervention. For the intervention to be possible, it is necessary to determine the feasibility of stent or stentgraft insertion into the vessel. Any location significantly occupied by plaques should be examined in this regard. Here, we propose a set of quantitative measures to formalize this examination in the future.

Lumen decrease factor. One of the measures is the Lumen Decrease Factor (LDF). This quantity, together with the plaque-free lumen area, indicates the site of a critical stenosis in the vessel tree. When the plaque area is separated from the lumen based, e.g., on the thresholding method presented in the previous subsection, the LDF can be calculated as

$$LDF = \frac{\text{lumen\_area}}{\text{lumen\_area} + \text{plaque\_area}}. \quad (15)$$

The analysis of the thresholding demonstrated a problem with interpretation of the part of the artery area located between the plaque and the artery wall. Pixels of this area have the intensity corresponding to the lumen and, as a result, their classification overestimates the LDF. Thus, before the calculation of this factor, it is necessary to correct the lumen area mask through elimination of such pixels. The following morphological formula can be used to detect these pixels located between the plaque and the artery wall:

$$[\delta_{SE}(BW_p) \cap BW_p^C] \cap [BW_a \cap (\epsilon_{SE}(BW_a))^C], \quad (16)$$

where δ and ϵ are the dilation and erosion, SE is the structuring element, BW_p and BW_a refer to the black-and-white masks of the plaque and the artery, and C refers to the image complementation. The type and size of SE, which is a parameter of the dilation and erosion, must be determined. We used a disk-shaped element with the radius of one pixel. An example of lumen and plaque area detection taking account of the above correction is presented in Fig. 3.

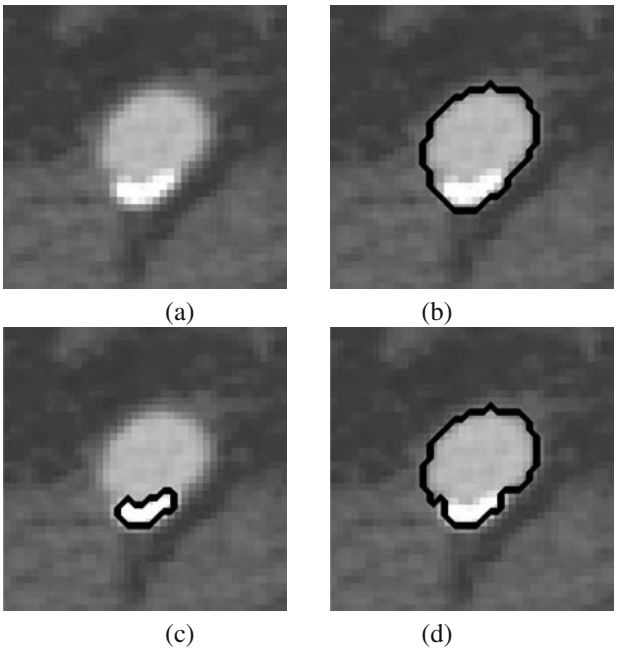

Fig. 3. Illustration of the problem of bordering between the plaque and the artery wall in CTA imaging: original image (a), recognized artery area (outlined by black) (b), segmented plaque area (outlined by black) (c) and corrected artery area according to Eqn. (15) (d). The narrow region between the plaque and the artery wall on the right and bottom sides was eliminated.

Circumference occupancy factor. The Circumference Occupancy Factor (COF) can be expressed as the portion of artery circumference occupied by atherosclerotic plaques. For image processing, the most adequate approach is to check for the presence of the plaques in different directions starting from the center of the artery cross-section. For this purpose, we used directions tilted by 5° each time to cover the full angle. The COF is calculated as follows:

$$COF = \frac{p_x}{72}, \quad (17)$$

where p_x is the number of radia that hit the plaques.

Owing to the problem of discretization, calculation of the COF is not a trivial task. Creation of a discrete representation of a radius with the selected direction requires selection of the radius length, determination of the pixels of the representation according to 4- or 8-point connectivity (e.g., based on the Bresenham algorithm), and comparison of the spatial distribution of the pixels with the plaque mask. This is not easy and we propose to invert this task by calculating the directions represented by the pixels of the plaque. However, because of the discrete representation of the plaque, the pixels identified by coordinates of their centers cover only some directions, as shown in Fig. 4(a). Labeling the plaques and analyzing them in the iteration process can solve this problem. For each plaque one can determine maximum and minimum angle directions of its pixels and then correct these values by half of the pixel size to cover all the directions in this range. After rounding to a set of 72 directions, the result of the determination of the directions pointing to the plaque is shown in Fig. 4(b).

Convex plaque area factor. To expand the description of the plaque position on the artery wall, we define the Convex Plaque Area Factor (CPAF), representing a ratio between the convex area of the plaque and the whole area of the artery cross-section. Thus, the CPAF can be calculated as follows:

$$CPAF = \frac{\text{convex\_plaque\_area}}{\text{artery\_area}}. \quad (18)$$

The convex plaque area is defined as the minimal convex polygon described on the plaque and obtained from the built-in Matlab function. This factor determines the part of the artery cross-section surrounded by plaque

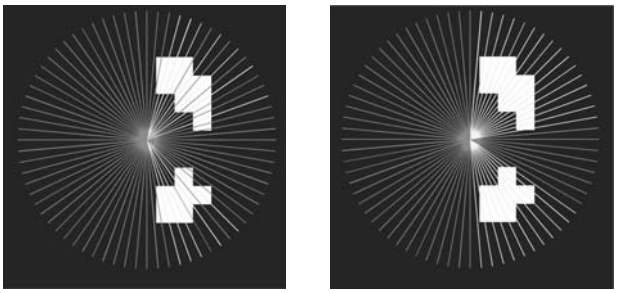

(a) (b)

Fig. 4. Illustration of the discretization problem in COF calculation. When only some directions (light grey) are covered by the coordinates of the pixel centers (a), using the extreme pixels from any plaque to cover the direction range gives a continuous result (b).

and indicates which part of the artery lumen may be inaccessible during potential intervention.

To illustrate the difference between the COF and CPAF, two cases are presented in Fig. 5. In case A (Fig. 5(a)), the COF and CPAF are similar (0.39 and 0.44, respectively), while in case B (Fig. 5(b)), COF equals 0.625 and the CPAF 0.92. In the latter case, the CPAF better describes the complexity of the plaque distribution.

Ellipse inscribed in the lumen area. During the planning of endovascular intervention, it is necessary to evaluate the artery lumen area in terms of its accessibility for the delivery system and stentgraft deployment. In view of the round shape of the system and possible adaptation of the artery wall, we propose to search for the highest ellipse inscribed in the lumen area.

One approach used in the detection of predefined shapes in binary images is the Hough transform. This transform is commonly used for determination of image lines based on the angular-distance representation of the discrete points. The obtained two-dimensional accumulative matrix is analyzed to find the local maxima corresponding to the existing lines. To detect the circular shape based on the Hough transform, the three-dimensional accumulative matrix is used or, as a more practical approach, a double Hough transformation of the image.

Finally, the transform can be used to detect the ellipses (Davies, 1989), but this requires advancing the 5-dimensional accumulative space which, obviously, is difficult to construct and analyze. This task can be divided into a few simpler steps and we have focused on the approach aimed at the direct detection of the inscribed ellipse. In this case, any pair of the antipodal points from the set of the object points is first taken into account. Such a pair uniquely defines the four parameters of the ellipse:

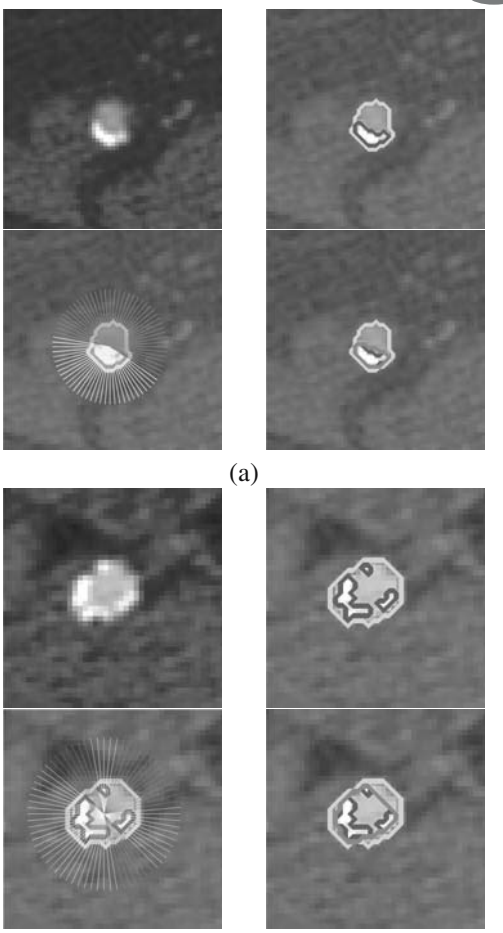

(a)

(b)

Fig. 5. Two examples to illustrate the difference between the COF and the CPAF. Upper left: original images, upper right: outlined whole artery (light grey line) and plaque (dark gray), bottom left: COF results with the bright radia pointing to the plaque and dark radia pointing to the plaque-free lumen, bottom right: CPAF with the plaque convex area outlined by medium grey bottom right.

center coordinates as well as the length and orientation of the major axis. Thus, only the length of the minor axis remains to be found. This way we obtained only the one-dimensional accumulative space which is calculated through the object points. To calculate this space, we used the ellipse equation in the form

$$\frac{x^2}{a^2} + \frac{y^2}{b^2} = 1. \tag{19}$$

The equation connects the dimensions of semi-axes a and b with coordinates of each ellipse point in the Cartesian system originating at the center of the ellipse. Coordinates of these points can be also defined by direction τ and distance d from the ellipse center as described below:

$$\begin{cases} x^2 = d^2 \cos^2 \tau, \\ y^2 = d^2 \sin^2 \tau. \end{cases} \tag{20}$$

Next, the cosine of the angle is defined by

$$\cos\tau = \frac{a^2 + d^2 - f^2}{2ad}, \tag{21}$$

where f is the distance from the ellipse point to the closest antipodal point. This set of equations leads to the formula for the semi-minor axis length

$$b = \sqrt{\frac{a^2 d^2 \sin^2\tau}{a^2 - d^2\cos^2\tau}}, \tag{22}$$

restricted by any ellipse point lying outside the end of the major axis.

The presented approach requires evaluation of the accumulative space simultaneously for any pair of the antipodal points and determination of its maximum. Comparison of this measure between the pairs allows us to find the ellipse with the highest accumulative value. However, this method is dependent on the image and accumulative space discretisations used, which may sometimes yield similar high accumulation values for the totally different ellipses (Fig. 6(a) and (b)), whereas for the ellipse which better fills out the object the accumulation value will be lower (Fig. 6(c)).

In this paper we propose to use another approach also based on pairs of the antipodal points. In this case, we calculate the maximum b value of the inscribed ellipse for any such pair based on the surrounding points which restrict the ellipse. In practice, these points can be obtained through dilation or, easier, by the extension of the object minimal window by one line in each direction. Recalculation of these points based on (21) and selection of the minimal value can be done. Due to the introduced reduction of a distance between the surrounding point and the ellipse centre by half of the pixel dimension, it is necessary to replace the original value with $d_r = d^2 - d + 0.25$. Instead of (21), the following formula should be used:

$$b = \sqrt{\frac{a^2 d_r^2 \sin^2\tau}{a^2 - d_r^2\cos^2\tau}}. \tag{23}$$

Finally, for each pair of the antipodal points we obtain the maximal b value. Comparison of the ellipse area between the pairs leads to the best result, as shown in Fig. 6(d).

3. Results

Based on the analyzed CT images we assessed the applicability of the methods of thresholding the artery area into the lumen and the plaque. We also compared the numerical results with the threshold value established manually by a team of experts composed of two vascular surgeons and a radiologist. For each slide, the threshold value was selected manually with the accepted final value to obtain the best segmentation results. To compare the

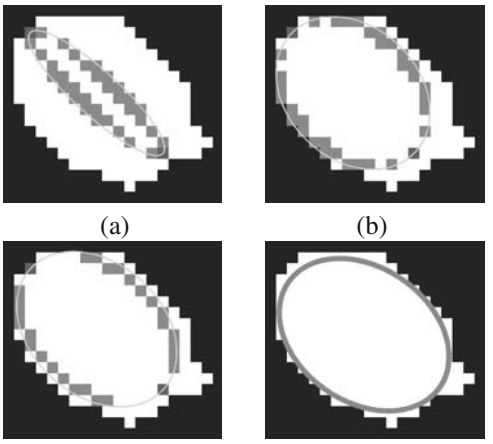

Fig. 6. Example of the detection of the maximal ellipse inscribed in the lumen area. Two results ((a) and (b)) with the highest accumulation value (equal to 32) based on the Hough transform give totally different results. The more appropriate result (c) has the value of only 16. For comparison, (d) shows the result obtained based on the pixel excluding criterion.

results, the level of the decreased lumen area in the artery cut-off plane was calculated. The mean absolute error of this measure and its standard deviation were calculated for the three artery segments: aortic, ilio-femoral and femoral.

These results are shown in Table 1. The following abbreviations were used: 1D and 2D—first and second derivative, GMM—Gaussian mixture modeling, GMM+R—Gaussian mixture modeling with linear regression, LLA—first derivative of the 11-fold local linear approximation, APX—12-th order polynomial approximation, APX+RMV—12-th order polynomial approximation with reduction of the minimum value, APX+DA—12-th order polynomial approximation with data averaging, CS—cubic spline, CS+DA—cubic spline with data averaging, S5+DA—spline of the 5-th order polynomial with data averaging, LSSS1—least squares smoothing spline ver. 1, LSSS2—least squares smoothing spline ver. 2, LSSS2+DA—least squares smoothing spline ver. 2 with data averaging, PCS6—piecewise cubic spline with six knots, PCS12—piecewise cubic spline with twelve knots, PCHIP—piecewise cubic Hermite interpolating polynomial, ERFIT—error function fitting.

The threshold values were calculated in two ways: (i) for a single image, and (ii) with averaging in the sequence of the CTA images. Upper indexes (in bold) indicate three methods which yielded results most closely corresponding to those obtained with the manual threshold evaluation. The results are presented graphically in Fig. 7. In the first case (a), the GMM detects a threshold value of 590, which results in the narrowest outline of the plaque. LLA detects a threshold of 515 and now the plaque is

Table 1. Mean absolute error of automatic estimation of the decreased lumen area relative to manual selection of the threshold value.

	Aorta		Ilio-femoral		Femoral	
Method	Single	With averaging	Single	With averaging	Single	With averaging
GMM	1.4 ± 1.1	$\mathbf{0.4 \pm 0.2^{1}}$	$\mathbf{1.9 \pm 1.3^{1}}$	$\mathbf{1.6 \pm 1.0^{1}}$	3.4 ± 4.3	2.0 ± 2.8
GMM+R	6.0 ± 3.0	2.1 ± 1.2	6.7 ± 5.5	4.4 ± 3.4	4.0 ± 3.4	1.7 ± 1.1
1D LLA	$\mathbf{1.3 \pm 0.3^{3}}$	$\mathbf{1.3 \pm 0.4^{3}}$	$\mathbf{2.0 \pm 0.6^{2}}$	2.4 ± 0.6	3.1 ± 1.7	4.1 ± 2.4
1D APX	3.1 ± 2.6	2.9 ± 2.6	7.2 ± 5.4	6.6 ± 5.2	2.6 ± 2.2	1.8 ± 1.3
1D APX+RMV	$\mathbf{1.2 \pm 0.8^{2}}$	2.3 ± 5.1	3.5 ± 1.9	$\mathbf{2.3 \pm 0.7^{3}}$	10.1 ± 8.1	14.3 ± 11.8
1D APX+DA	3.1 ± 2.6	2.9 ± 2.6	7.3 ± 5.4	6.6 ± 5.3	2.7 ± 3.4	2.1 ± 2.5
1D CS	3.5 ± 2.9	3.2 ± 2.8	7.6 ± 5.6	6.9 ± 5.4	2.2 ± 1.9	1.7 ± 1.2
2D CS+DA	3.6 ± 3.0	3.3 ± 2.9	7.7 ± 5.8	7.0 ± 5.6	$\mathbf{1.5 \pm 1.6^{3}}$	$\mathbf{1.4 \pm 1.2^{3}}$
2D S5+DA	2.6 ± 2.3	2.3 ± 2.1	5.8 ± 4.2	5.2 ± 4.3	2.1 ± 1.8	1.6 ± 1.1
1D LSSS1	3.5 ± 2.8	3.2 ± 2.8	7.5 ± 5.6	6.8 ± 5.3	2.3 ± 2.0	1.8 ± 1.3
1D LSSS2	3.3 ± 2.7	3.0 ± 2.7	7.4 ± 5.5	6.7 ± 5.3	3.1 ± 4.1	2.7 ± 3.5
1D LSSS2+DA	3.0 ± 2.6	2.9 ± 2.6	7.1 ± 5.5	6.5 ± 5.3	$\mathbf{1.4 \pm 1.4^{2}}$	$\mathbf{1.3 \pm 1.0^{2}}$
1D PCS6	3.2 ± 2.8	3.0 ± 2.8	7.3 ± 5.5	6.7 ± 5.4	4.1 ± 6.0	3.5 ± 6.0
1D PCS12	3.0 ± 2.5	2.8 ± 2.5	7.1 ± 5.3	6.5 ± 5.2	2.6 ± 2.3	1.9 ± 1.4
1D PCHIP	3.5 ± 2.9	3.2 ± 2.8	7.6 ± 5.6	6.9 ± 5.4	2.3 ± 2.1	1.7 ± 1.3
1D B-spline	3.5 ± 3.0	3.2 ± 2.9	7.6 ± 5.7	6.9 ± 5.5	1.7 ± 1.6	$\mathbf{1.4 \pm 1.2^{3}}$
1D ERFIT	$\mathbf{1.0 \pm 0.6^{1}}$	$\mathbf{0.8 \pm 0.9^{2}}$	$\mathbf{2.4 \pm 1.7^{3}}$	$\mathbf{2.1 \pm 1.5^{2}}$	$\mathbf{0.9 \pm 0.6^{1}}$	$\mathbf{1.3 \pm 0.7^{1}}$

the widest. APX+RMV and ERFIT detect the values of 540 and 520, respectively, associated with intermediary plaque areas. In the second case (b), GMM-thresholding also produces the most limited results (threshold value of 564), while the remaining methods detect the value of 545 and, consequently, more precisely determine the outline of the plaque. However, the latter result includes some small errors on the right side of the artery area. The last case (c) is the most problematic due to the ambiguous imaging flow in the artery resulting from the complete artery blocking by the plaque located just below the test site. The obtained threshold values are 378 (GMM), 675 (LLA), 688 (APX+RMV), and 702 (ERFIT). This case may be difficult to assess not only automatically, but also manually, and the only conclusion is that the GMM overestimates the plaque area.

The results suggest that no single method can perfectly estimate the threshold value for all the investigated regions of the artery. Also, averaging the threshold value in the CT images sequence has a huge impact on the precision of thresholding. However, our results also indicate that only six methods provide data highly compatible with those of the manual analysis. In the single threshold estimation approach, ERFIT provided the most promising results for the aorta and femoral artery regions, whereas the GMM faired better for the ilio-femoral region. Slightly better results were obtained using threshold averaging. With the use of the GMM method, especially in the aorta region, the mean error decreased from 1.4 to 0.4%. However, in the case of the femoral region, threshold averaging decreased the efficiency of the ERFIT method with the error increasing from 0.9 to 1.3%. Overall, the best results were obtained

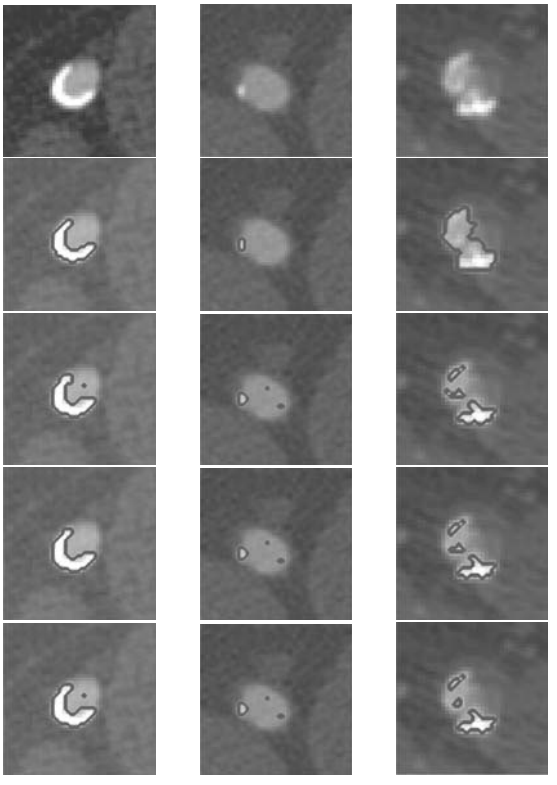

(a) (b) (c)

Fig. 7. Example of the thresholding results for three arteries (a), (b) and (c). The images from up to down represent the original image, GMM-based thresholding, LLA, APX+RMV and ERFIT methods. The recognized plaques are outlined in dark gray.

Table 2. Computational time of the various methods.

	Computational time [s/100 scans]		
Method	Aorta	Ilio-femoral	Femoral
GMM	2.2771	1.7076	1.2211
GMM+R	10.2928*	22.0853*	14.8367*
1D LLA	52.0237	25.4644	14.6024
1D APX	0.1336	0.1267	0.1231
1D APX+RMV	0.1380	0.1306	0.1260
1D APX+DA	0.1738	0.1680	0.1622
1D CS	0.1322	0.1095	0.0986
2D CS+DA	0.3046	0.2683	0.2320
2D S5+DA	0.3435	0.2924	0.2500
1D LSSS1	0.5442	0.4306	0.3678
1D LSSS2	0.2039	0.1501	0.1258
1D LSSS2+DA	0.2607	0.2078	0.1757
1D PCS6	6.7916	6.9502	6.4700
1D PCS12	6.3104	5.8039	6.0117
1D PCHIP	0.0742	0.0665	0.0619
1D B-spline	4.4339	4.3915	4.3589
1D ERFIT	88.2609	55.9565	32.1552

*divergent results

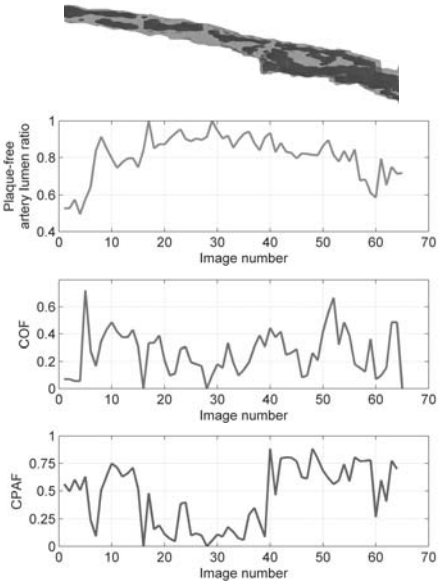

Fig. 8. Example of artery reconstruction and measures obtained for patient 1. First, there is a 3D reconstruction of the artery lumen (light) with plaques (dark). Below them, three plots represent the factors under consideration: the LDF, COF and CPAF through the 66 scans.

for the aorta and ilio-femoral regions analyzed with use of the GMM with threshold averaging, and for the femoral region with the use of ERFIT without the averaging.

Another important practical issue is the time of computation. In all the methods, the time of estimation of the threshold for one hundred randomly selected images was measured with a 2.80 GHz Core Duo, 4GB RAM PC. The results are shown in Table 2. As indicated, the computational time of the aorta images was, depending on the method used, 1.1- to 3-fold longer than the time of computation of the femoral artery. This prolongation resulted from the larger area of the analyzed artery cut-off plane and, consequently, the larger number of the data. The number of the pixels averaged over the aorta images was 539, while the ilio-femoral region had, on average, 289 pixels and the femoral region—184 pixels. To recapitulate, among the methods we use polynomial approximations were associated with the shortest time of computation. In contrast, owing to optimization of the solution of the constrained linear least squares problem, the definition of which is necessary to obtain the monotonical function, the ERFIT method took the longest to compute the threshold value. To accelerate this process, we can use a fixed number of knots and coefficients from the previous image analysis in the artery tracking process as an initial vector in optimization. Next, the algorithms addressed to solve the constrained linear least squares problem with non-negative coefficients can be selected instead of the default ones. Such tricks allow us to reduce the time of computation by almost 90%.

From the interventional point of view, in addition to proper plaque recognition and 3-D visualization, the factors described Section 2.4 are of utmost importance. To illustrate changes and differences between these factors along the course of the artery, two sample cases are presented in Figs. 8 and 9. In both arteries the occurrence of plaques varied widely from no plaques at all to the whole artery wall being covered by them. In patient no. 1 only 20% of the lumen of the analyzed artery was occupied by plaques. However, in scans no. 10–15 and 40–60 the CPAF values were high, indicating an increased risk of endovascular intervention. Obviously, this measure better than others indicates unfavourable arrangement of plaques. In patient no. 2 (registered with the highest z resolution) the CPAF also properly indicated problematic sites in scans 10–30, 70–90, 185–215, and 260–270. The highest occupation (about 45%) of the lumen by plaques was found in scan no. 185, whereas the lowest COF value was determined for scan no. 5. These differences suggest that all the measures should be analyzed together. Their practical clinical value will be estimated in future studies.

4. Discussion

Numerical description of arterial vessels based on advanced imaging aided with appropriate computer methods is one of the most interesting and promising trends in medical image processing. Currently, numerical evaluation of selected parts of the vessels is conducted mostly manually based on a single CTA image. A

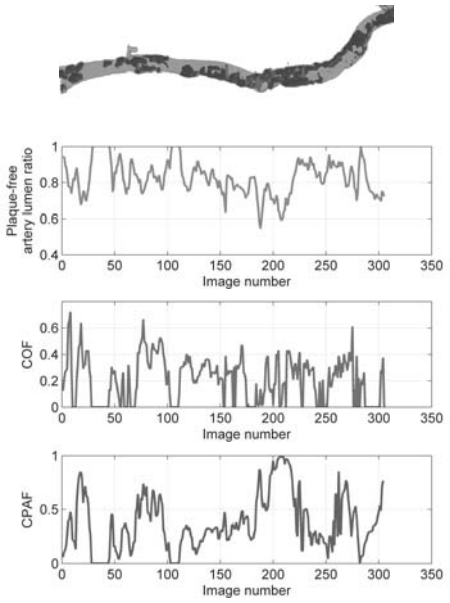

Fig. 9. Example of artery reconstruction and measures obtained for patient 2. First, there is the 3D reconstruction of the artery lumen (light) with plaques (dark). Below them, three plots represent the factors under consideration: the LDF, COF and CPAF through 306 scans.

common system for the quantitative evaluation of atherosclerotic changes in the iliac and femoral arteries applicable to the sequence of the CTA images is still under elaboration. The lack of such a system significantly limits our capacity to assess blood flow in vessels and impedes diagnostic efficacy for patients with cardiovascular diseases.

In the present study, we describe and compare a set of numerical and statistical approaches to the problem of differentiation between the vessel lumen and the atherosclerotic plaques. A crucial step in this process is to make a precise quantitative evaluation of the plaques, both locally and along the longer course of the artery. Results of the analysis of the distribution curve of the sorted intensities of the pixels suggest that the boundary between the lumen and the plaque intensity is at the bending point on this curve. This observation inspired us to use linear fitting methods and the derivatives of the obtained functions for counting of the threshold value.

In our study we used a pixel intensity graph which is arranged inversely to the cumulative distribution. This was necessary because only the polynomial approximation of such a function is possible with acceptable accuracy. The polynomial approximation of the cumulative distribution cannot be established because the distribution approaches a limit when the argument increases, which is incompatible with the character of polynomials.

Notably, as demonstrated by our own preliminary results indicating local value changes in the pixels distribution curve, application of differential rules such as the Gear rules is not useful for estimating the derivatives. Hence, we used polynomial approximation, spline functions, and other fitting methods. We are aware that the 12-th polynomial approximation is associated with the ill-conditioned system of linear equations, but can still be successfully solved by Matlab functions. The default algorithm was based on the Vandermonde matrix and application of the QR method to abscissa-normalized data.

The obtained results confirm that some of the investigated methods are better than others. The best results were obtained with statistical Gaussian mixture models and with numerical error function fitting. The latter method, both with and without threshold value averaging, appeared to be one of the top three best suited methods for examination of all the investigated arterial regions. There are two possible reasons why Gaussian mixture models yielded higher errors during examinations of the femoral artery. Firstly, this artery has a smaller cut-off plane area and the dominant of the lumen intensity representation is lower compared to the other investigated arterial regions. Consequently, worse fitting of the Gaussian distribution is obtained. Secondly, femoral arteries are thinner and more peripheral in the arterial tree, resulting in less homogeneous distribution of the contrast medium in the vessel lumen, as shown by cases (e3) and (f3) in Fig. 2. In these cases, the segments of the distribution curves refer to the lumen areas which have steeper slopes than the ones obtained for cases (a) to (d).

In terms of computational time, both the GMM and ERFIT appeared to be rather slow: compared with the fastest least squares approximation methods, the former was about ten times slower and the latter, the most time-consuming algorithm, was 30–40 times slower than GMM. The constrained linear least squares solver is a crucial part of ERFIT, occupying almost 90% of the total computational time. In the case of constrained linear least squares optimization called 300 times the tricks described in Section 3 may decrease the time of computation from about 217 sec to only 17 sec. This way, the ERFIT method can be used without significantly increasing the time of the analysis.

Quantification of atherosclerotic changes in an artery is not a trivial task. Determination of the most useful factors for prediction of possible problems in endovascular intervention requires application of various measures capable of adequate evaluation of the investigated artery lumen and plaque arrangement. None of the parameters described so far can perfectly differentiate between different stages of an atherosclerotic alteration. In this paper we introduced and analyzed two such parameters: the convex plaque area factor and the circumference occupancy factor. The presented results

show the differences between and the usefulness of the proposed measures. Also, a practical approach to the detection of the maximum elliptic area inscribed in the artery lumen was proposed. We suggest that the centre of the ellipse be used as an initial point for calculation of the COF. Each of the factors used differently describes the observed atherosclerotic changes, but only information provided by all of them can be used to objectively assess the investigated alterations.

5. Conclusion

In conclusion, the obtained results of the simulations indicate that, depending on the arterial tree and the expected time of the analysis, two methods can be efficiently used for differentiation between the plaque and the lumen: one of them (GMM, especially with threshold value averaging) can be recommended for the analysis of the aorta and the ilio-femoral artery, another (ERFIT)—for the assessment of the femoral artery. However, the data shown in Table 2 and discussed by us suggest that there is no gold standard at present for unequivocal differentiation between the vessel lumen and the atherosclerotic plaques.

During intervention planning, various indicators of the state of the arteries should be considered. In addition to the obvious estimation of the plaque-free artery lumen, we introduce here two novel measures: the COF and the CPAF. The former parameter defines to what extend the artery circumference is occupied by the calcified plaque: firstly, it provides information about the quality of artery wall and, secondly, estimates the possibility of the artery wall extension which is responsible for artery adaptation for manipulation during the intraluminal intervention. The value of this measure higher than 0.5 seems to be critical in terms of artery wall elasticity. In this case, the surgeon must be aware that only the free lumen of the artery is accessible and that such procedures as, e.g., predilatation should not be performed.

The CPAF defines the spatial distribution of an atherosclerotic plaque around the artery lumen. It informs what part of the lumen can be poorly accessible for endovascular tools. When the plaques are located only on one side of the lumen, the tool penetrates the artery easier than when the plaques are located on different lumen sides. We assume that the CPAF value higher than 0.6 indicates an unfavourable situation.

The examination of arteries proposed in the present study is based on long-term experience from and observations carried out during low-invasiveness surgical procedures. The cut-off values of the defined parameters proposed by us for such examinations are only preliminary and should be verified in future investigations.

References

Adame, I.M., van der Geest, R.J., Wasserman, B.A., Mohamed M.A., Reiber, J.H. and Lelieveldt, B.P. (2004). Automatic segmentation and plaque characterization in atherosclerotic carotid artery MR images, *MAGMA* **16**(5): 227–234.

Andrews, L.C. (1997). *Special Functions of Mathematics for Engineers*, SPIE Press, Bellingham.

Davies, E.R. (1989). Finding ellipses using the generalised Hough transform, *Pattern Recognition Letters* **9**(2): 87–96.

De Boor, C. (2001). *A Practical Guide to Splines (Revised Edition)*, Springer, New York, NY/Heidelberg.

Demirkaya, O., Asyali, M.H. and Sahoo, P.H. (2009). *Image Processing with MATLAB: Applications in Medicine and Biology*, CRC Press, Boca Raton, FL.

Frąckiewicz, M. and Palus, H. (2011). KHM clustering technique as a segmentation method for endoscopic colour images, *International Journal of Applied Mathematics and Computer Science* **21**(1): 203–209, DOI: 10.2478/v10006-011-0015-0.

Fritsch, F.N. and Carlson, R.E. (1980). Monotone piecewise cubic interpolation, *SIAM Journal of Numerical Analysis* **17**(2): 238–246.

Kerwin, W., Xu, D., Liu, F., Saam, T., Underhill, H., Takaya, N., Chu, B., Hatsukami, T. and Yuan, C. (2007). Magnetic resonance imaging of carotid atherosclerosis: Plaque analysis, *Topics in Magnetic Resonance Imaging* **18**(5): 371–378.

Manniesing, R., Velthuis, B., van Leeuwen, M., van der Schaaf, I., van Laar, P. and Niessen, W. (2006). Level set based cerebral vasculatural segmentation and diameter quantification in CT angiography, *Medical Image Analysis* **10**(2): 200–214.

Manniesing, R., Viergever, M. and Niessen, W. (2007). Vessel axis tracking using topology constrained surface evaluation, *IEEE Transactions on Medical Imaging* **26**(3): 309–316.

Manniesing, R., Viergever, M., van der Lugt, A. and Niessen, W. (2008). Cerebral arteries: Fully automated segmentation from CT angiography—a feasibility study, *Radiology* **247**(3): 841–846.

Manniesing, R., Schaap, M., Rozie, S., Hameeteman, R., Vukadinovic, D., van der Lugt, A. and Niessen, W. (2010). Robust CTA lumen segmentation of the atherosclerotic carotid artery bifurcation in a large patient population, *Medical Image Analysis* **14**(6): 759–769.

Piegl, L. and Tille, W. (1997). *The Nurbs Book*, Springer, New York, NY/Heidelberg.

Renard, F. and Yang, Y. (2008). Image analysis for detection of coronary artery soft plaques in MDCT images, *5th IEEE International Symposium on Biomedical Imaging (ISBI '08), Paris, France*, pp. 25–28.

Soille, P. (2003). *Morphological Image Analysis, Principles and Applications (Second Edition)*, Springer, Berlin.

Stoer, J. and Bulirsch, R. (2010). *Introduction to Numerical Analysis*, Springer, New York, NY/Heidelberg.

Vukadinovic, D., Rozie, S., van Gils, M., van Walsum, T., Manniesing, R., van der Lugt, A. and Niessen, W.J. (2012). Automated versus manual segmentation of atherosclerotic caroid plaque volume and components in CTA: Associations with cardiovascular risk factors, *International Journal of Cardiovascular Imaging* **28**(4): 877–887.

Vukadinovic, D., van Walsum, T., Manniesing, R., Rozie, S., Hameeteman, R., de Weert, T., van der Lugt, A. and Niessen, W. (2010). Segmentation of the outer vessel wall of the common carotid artery in CTA, *IEEE Transactions on Medical Imaging* **29**(1): 65–76.

Yang, F., Holzapfel, G., Schulze-Bauer, C., Stollberger, R., Thedens, D., Bolinger, L., Stolpen, A. and Sonka, M. (2003). Segmentation of wall and plaque in in vitro vascular MR images, *International Journal of Cardiovascular Imaging* **19**(5): 419–428.

Yang, Y., Huang, S. and Rao, N. (2008). An automatic hybrid method for retinal blood vessel extraction, *International Journal of Applied Mathematics and Computer Science* **18**(3): 399–407, DOI: 10.2478/v10006-008-0036-5.

Tomasz Markiewicz (Ph.D.: 2006, doctor habilitatus: 2011) is an associate professor at the Electrical Engineering Faculty, Warsaw University of Technology, and a specialist in the Department of Pathomorphology, Military Institute of Medicine, Warsaw, Poland. His primary research and practical tasks are related to medical image and signal processing. He has been recently involved in histological image analysis in pathomorphology, applied mathematical morphology, texture analysis, feature selection, and neural networks in classification tasks. In 2011 he was elected a member of the Young Scientist Academy, Polish Academy of Sciences.

Mirosław Dziekiewicz (M.D., Ph.D.: 1999) is a deputy head at the Department of Vascular and Endovascular Surgery, Military Institute of Medicine, Warsaw, Poland. He specializes in surgical endovascular and hybrid procedures. Recently, he has been engaged in optimization of vascular access for endovascular intervention in patients with arterial diseases including surgical trauma, atherosclerosis, aneurysms and other pathologies.

Romana Bogusławska-Walecka (M.D., Ph.D.: 1989, doctor habilitatus: 1997, full professor: 2011) is the head of the Department of Radiology, Military Institute of Medicine, Warsaw, Poland. She specializes in imaging in neuroradiology. Her recent work focuses on contrast-induced nephropathy and diagnostic values of multislice computed tomography as well as magnetic resonance of head and neck cancer.

Marek Maruszyński (M.D., Ph.D.: 1978, doctor habilitatus: 1985, full professor: 1996) is the head of the Department of Vascular and Endovascular Surgery, Military Institute of Medicine, Warsaw, Poland. He specializes in surgical endovascular and hybrid procedures. His recent work focuses on vascular surgery in patients with surgical trauma, genetics of atherosclerosis, and minimally invasive surgery.

Wojciech Kozłowski (M.D., Ph.D.: 1978, doctor habilitatus: 1995, full professor: 2005) is the head of the Department of Pathomorphology, Military Institute of Medicine, Warsaw, Poland. He has recently concentrated on immunohistology significance in different cancer diagnosis and prognosis, the role of immunohistology in the diagnosis and prognosis of primarily gastrointestinal cancer as well as on histological image analysis in pathomorphology.

Received: 4 January 2013
Revised: 30 August 2013